Proceedings of the 2009 IEEE International Conference on Systems, Man, and Cybernetics
San Antonio, TX, USA - October 2009

Radioscopic Inspection of Cargo Containers with Megavoltage Energy Barriers

Ajay K. Mandava, Lei Zhang, Emma E. Regentova
Electrical and Computer Engineering
University of Nevada, Las Vegas
4505 Maryland Parkway, Box 454026
Las Vegas, NV 89154-4026

Zane Wilson, Gongyin Chen
Varian Medical Systems, Inc.
Security & Inspection Products
6811 Spencer Str., Las Vegas, NV 89119

***Abstract*—To perform the inspection of cargo containers the radioscopic screening is performed by switching between 6 and 9 MeV of boundary energies as rapidly as 200 times per second and measuring the penetration levels in the contents of cargo. This technology facilitates the material identification via the analyses of the ratios of signals obtained at nominal and dual energies, which are 6 and 9 MeV, respectively. The techniques are developed for (a) visualizing the contents to produce an image suitable for fast inspection by a human operator, and for (b) prompting the custom personnel about the location of suspicious objects. Specifically, nuclear materials are of interest. The experiments have been conducted with Linatron K9 device designed by Varian Security and Inspection Products [1]. The capabilities are demonstrated for detection of objects of interests for the steel shields of 10 inches of thickness.**

***Keywords*—Dual Energy X-Ray, Cargo Imaging, Material Discrimination**

I. INTRODUCTION

Currently the nation faces a threat that terrorists will attempt to smuggle weapons of mass destruction (WMD) through the border. Most likely, this will be a device that combines radioactive materials with conventional explosives to make a radiological dispersion device [2]. Thus, it is important to detect the transport of nuclear or radiological materials. However, of the seven million cargo containers that arrive through U.S. seaports every year, an extremely small percentage, i.e., 5-6% are ever examined because of the labor involved to physically open each container, extract and inspect the contents [3]. This is very time consuming and even unrealistic under the real-time constrain.

Advanced dual-energy X-ray cargo inspection systems can play a crucial role in ensuring national security by providing a real-time inspection of cargos advancing through the customs. It is evident that both the speed and the robustness of the procedure are to be addressed and secured. In other words the inspection must support a smooth flow of goods through the border without obstructing the traffic. Also, the technology is responsible for provisioning the accuracy in screening the contents. Transformed into the system properties, this means that a fast screening procedure featured by a low false positive rates and a high true positive detection of threats or contraband is expected.

Threatening material and its container are characterized by high atomic numbers. Normally, cargo does not generally exceed iron or copper in atomic numbers (Z = 26 or 29). Important elements sought as threats or their shields are ^{90}Th, ^{92}U, ^{94}Pu, ^{82}Pb and ^{74}W [1].

Multiple-energy level radioscopic imaging allows for determining the make-up of scanned objects by exploiting differences in how the material interacts with X-rays at different energies [4]. The process involves taking two X-ray projection images of the same object using X-ray spectra with different end point energies and extracting information about the atomic number, Z of the material using the ratio of the attenuation levels. This is possible because at some energy X-ray interacts via two different physical mechanisms related to the atomic number of the scanned material [5][6].

The exponential law of the attenuation of the gamma radiation is defined as a ratio of logarithmic transparencies at nominal and dual energies. It characterizes the material of the barrier irrespective to its thickness. The above mentioned law forms a physical principle of the material discrimination.

The radioscopic transparency of a material with a mass thickness t and an atomic number Z , absorbtion coefficient μ for a bremsstrahlung beam with boundary energy E_e is expressed as a ratio of the radiation intensity before and after the penetration through the barrier:

$$T(E_e,t,Z)=\frac{\int_0^{E_e}\frac{dp}{dE_\gamma}(E_e,E_\gamma)e^{-\mu(E_\gamma,Z)}dE_\gamma}{\int_0^{E_e}\frac{dp}{dE_\gamma}(E_e,E_\gamma)dE_\gamma} \quad (1),$$

where the integrand function is a product of bremsstrahlung intensity according to the Schiff formula [7] and the detector response factor [8]:

$$\frac{dp}{dE_\gamma}(E_e,E_\gamma)=\frac{dI}{dE_\gamma}(E_e,E_\gamma)\left(1-e^{-\mu_{\det}(E_\gamma)t_{\det}}\right)\frac{\mu_{\det}^{en}(E_\gamma)}{\mu_{\det}(E_\gamma)} \quad (2)$$

Usually, the solution of a system cannot be found in general terms, as the barrier can represent a heterogeneous mixture of materials. As such, a number of unknown variables might exceed the number of equations. Two transparency profiles during irradiation of a barrier with nominal and dual boundary energies can be obtained, while atomic number and mass

978-1-4244-2794-9/09/$25.00 ©2009 IEEE

thickness of a material can be evaluated as a solution of a system of integral equations [9].

In order to ascertain the possibility of discrimination according to Z it is useful to introduce a ratio, R of logarithmic transparencies (inverse value of absorption) at the nominal E_1 and dual E_2 boundary energies of bremsstrahlung:

$$R(E_1, E_2, t, Z) = \frac{\ln(E_1, t, Z)}{\ln(E_2, t, Z)} = \frac{\overline{\mu}_{eff}(E_1, t, Z)}{\overline{\mu}_{eff}(E_2, t, Z)} \qquad (3)$$

For monochrome gamma beam, R in (3) is defined as a ratio of the total absorption coefficients at the nominal and dual energies. R is a constant and it uniquely characterizes the irradiated material.

One of the polychromatic X-ray spectra must be at a high enough energy so that the pair production accounts for much of the attenuation. Typically 9 MeV is sufficient for this purpose. The other spectrum should be at an energy level that is significantly lower. However, since the X-ray drops as the energy level decreases, it is impossible to select an energy level that is too low [4]. We used 6 MeV in the experiments which represents a good compromise between the energy and flux. Under the selected levels a library of R values can be obtained and further used for a table look-up for identification. The technology however allows to single material or a group of materials belonging to a cluster of close atomic numbers.

Although the system is required to be automated at a possibly large extent, the visual observation must take place concurrently. We see the possibility of invoking two lines of detection in parallel. The automaton points to the location of a possible threat. The operator is supplied with a tool of examining the image and manipulating it such that a better quality of an area of interest is obtained and enhanced in various ways for examination. The system also relates the type of the material and the shape of the suspicious object to make the prompting decision. The above described technology poses many challenges. Among the problems one encounters a scatter noise generated by the device and the container, a low resolution related to the distance to the objects to be scanned, the clutter nature of the container and the possibility of hiding the objects by shielding them wisely. The analysis of heavily loaded containers with materials of similar atomic numbers is certainly a difficult and a time consuming task, specifically if additionally the shape recognition is involved.

In this paper, we present a new approach to the image analysis and processing in which we combine a set of techniques for image enhancement, segmentation, and visualization and material identification. Based on the result of such processing, the material discrimination can be implemented more efficiently. The device used in the system is the Linatron-K9 developed by Varian Medical and Security Products Initial experiments have shown that device can penetrate through 440 mm (17 inches) of steel. By alternating between 6 and 9 MeV beams, a pair of 16-bit images is produced. The image processing is involved for analyzing the pair of images and prompting he operator on the presence of any "suspicious" objects according to the absorption at 9 MeV boundary energy and a ratio of two end-point energy penetrations. An area of interest is presented to the operator in a form suitable for the visual analysis.

The paper is organized as follows; the second section introduces the methods used for visualization and the material discrimination. In the third section the experiment and results are described; then follows Discussion. Conclusions are drawn in the last section of the paper.

II. Visualization and Material Identification

An image produced by 9 MeV X-ray penetrations is segmented. This allows for extracting objects of high atomic numbers, such as W, Pb and DU, as well as areas containing thick steel components. Then the ratio R of two end-point energy signals is calculated for the objects resulted from segmentation; shapes are analyzed for identified objects of interest and decision is made and presented to the operator.

The container is extracted from the background and the cabin and track are "removed" from the further processing pipeline. This allows for saving processing time and avoiding any confusion if alike materials are found outside the container, for example is the engine. The subtraction is performed using the intensity profile calculation. The basic principle employed in finding the vertical and horizontal profile is accumulation in each column, and in each row, respectively, and in finding the points of global drops indicating lowest penetration points.

Further steps involve median filtering and the logarithmic scaling. The former is performed for smoothing the high frequency noise due to the scatter. This step is important for the ease of segmentation procedure and a better approximated mean ratio value of absorption levels for the object at the later step.

The logarithmic scaling is needed for the human operator, and it is simply performed by the conversion

$$s = c \times \log(r + 1) \qquad (4),$$

where c is a fixed scaling constant,

$$c = \frac{\max(I)}{\log(1 + |r|)} \qquad (5),$$

and max(I) is the maximum intensity of the pixel; r is the value of the input pixel and s is the corresponding value of the output pixel.

The next step involves segmentation based on the fuzzy C-means (FCM) clustering method. The FCM algorithm is an iterative procedure that finds clusters in data by exploiting the concept of fuzzy membership: instead of assigning a pixel to a single cluster, each pixel is assigned different membership values on each of groups. This is done by minimizing an objective function J,

$$J = \sum_{i=1}^{N} \sum_{j=1}^{C} \mu_{ij}^{m} \left| x_i - c_j \right|^2 \qquad (6)$$

where

$$c_j = \frac{\sum_{i=1}^{N} \mu_{ij}^m x_i}{\sum_{i=1}^{N} \mu_{ij}^m} \tag{7}$$

$$\mu_{ik} = \frac{1}{\sum_{k=1}^{C} \left(\frac{|x_i - c_j|}{|x_i - c_k|} \right)^{\frac{2}{m-1}}} \tag{8}$$

If after one iteration of the algorithm the value of J is smaller than before it means the algorithm is converging or getting closer to a good separation of pixels into clusters; N is the number of pixels in the image; C is the number of clusters used in the algorithm; μ is the membership table of N×C entries which contains the membership values of each data point and each cluster; m is a fuzziness factor (a value larger than 1); x_i is the i^{th} pixel in N, c_j is j^{th} cluster in C; $|x_i\text{-}c_j|$ is the Euclidean distance between x_i and c_j.

The procedure is as follow.

Step 1: Initialize μ as a random value between zero and one; but with the sum of all fuzzy membership table elements for a particular pixel being equal to 1.

Step 2: Calculate a first value for J using (6).

Step 3: Calculate the centroids of the clusters c_j using (7).

Step 4: Calculate the fuzzy membership table using (8).

Step 5: Recalculate J according to (6).

Step 6: Go to step 4) until the stopping condition is reached.

The process stops when either a given number of iterations is executed in which we can consider that the algorithm achieved a 'good enough' clustering, or the difference between the values of J in consecutive iterations is smaller than a specified parameter ε, which indicates the convergence.

The segmented image is further analyzed by calculating the mean R values and looking up in the table for material mapping.

For visualization purpose, a new synthetic image is created with pseudo-colors. Each object is marked with a color based on the average intensity value. We apply the intensity slicing coloring. All pixels in the image are sliced into seven groups based on their intensity values, and then assigned color based on their group numbers and intensity value according to the following equations:

$$G(m) = \left\{ p \left| \frac{(m-1)P_{\max}}{9} < p < \frac{mP_{\max}}{9} \right. \right\} \qquad m = 1,2,\cdots,7$$

$$m(p) = \left(m = m_i, if \quad \frac{(m_i - 1)P_{\max}}{7} < p < \frac{m_i P_{\max}}{7}, m_i \in (1,2,\cdots,7) \right)$$

$$index(p) = 256 \times \left[\frac{7p}{P_{\max}} - (m(p) - 1) \right]$$

$$R(p) = index(p) \quad m(p) = 1,4,5,7$$

$$G(p) = index(p) \quad m(p) = 2,4,6,7$$

$$B(p) = index(p) \quad m(p) = 3,5,6,7$$

where P_{max} is the maximum intensity of the image (P_{max} is 65535), $G(m)$ is the m^{th} group of pixels, $m(p)$ is the group number of pixels with intensity value of p, $index(p,m)$ is the color index of pixels with intensity value of p, and $R(p)$, $G(p)$, $B(p)$ are color indexes of pixels with intensity value of p in red, green and blue color.

III. EXPERIMENTS

The Linatron K9 (based on a klystron) developed by Varian is used in the experiments. The X-rays are produced in the device's target made from tungsten. It absorbs high energy electrons and produces X-rays. The target is designed to produce a minimum focal spot size consistent with its high radiation output. Depending on the energy of individual photons three processes contribute to the aggregate attenuation f of the beam, i.e. photoelectric absorption, when photon moves through the material with a high speed, Compton scattering, when photon is deflected from its initial line of travel and moves in different directions with a lower speed, and pair production characterized by the complete absorption and creation of electron-positron pair.

High-energy X-ray photons generated by the device are absorbed and scattered in varying amounts by the materials in their path, depending on their densities and atomic structure. On the far side of the cargo container, a linear CdWO detector collects and records the photons passed through unabsorbed or unscattered, generating an electronic signal that is translated into an image. The outline of the imaging chain containing the device is shown in Fig. 1. Two sets of collimators are used for the maximum scatter control and to narrow the beam to the detector area.

To test the capabilities of the device and obtaining the library values for ratio, R of absorption levels at boundary energies, we have used a few materials of interest whose properties are listed in Tab. 1. The objects are slabs of 1cm×5cm×20cm. All cubes 100 cc (DU is overcoated). They have been placed in three levels steel plate stack as explained in Tab. 2. The DRs have 1 mm sampling with non-square pixels and 3.0 ms integration time. The DR range is 250 to 0 mm to allow an oversize DU cube on the top. A steel plate stack is located near beam line. The gain calibration has empty frame in place. Calibration is performed as for at roughly 680 rad/min 6 MEV and at roughly 2900 rad/min for 9 MeV energy.

An example of 9MeV image with a 6" steel plate shield is shown in Fig. 2(a). The image resulted from the segmentation based on the set of procedures explained in Section II, with a median filter of size 3 is displayed in Fig. 2(b). The parameters of FCM are set as follows: C = 5; m = 2; maximum iteration is 50.

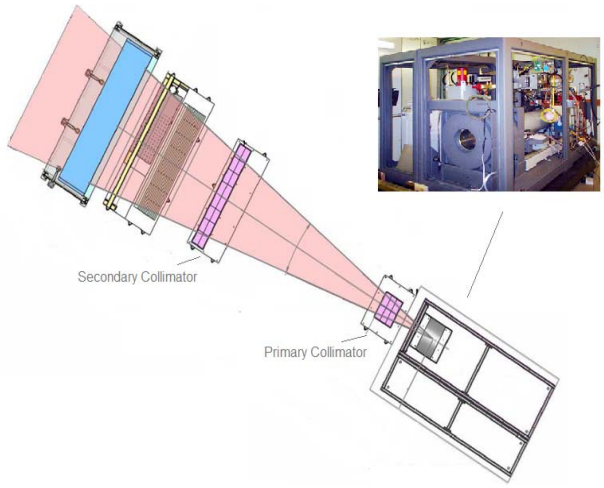

Figure 1. Linatron-K9 in the imaging chain

TABLE I. ELEMENT PROPERTIES OF SOME MATERIALS

Chemical symbol	**Al**	**Sn**	**Fe**	**Pb**	**W**	**DU**
Name of element	Aluminum	Tin	Iron	Lead	Tungsten	Depleted Uranium
Atomic number	13	50	26	46	74	92
Density(g/cm^3)	2.669	7.31	7.874	12.02	19.30	18.95
Mass Attenuation Coefficients (Z/A)*	0.48181	0.42120	0.46556	0.43225	0.40250	0.38651
Relative atomic mass	10.811	118.710	55.845	106.42	183.84	238.029

* X-ray mass attenuation coefficient values are given for the ratio, R of atomic number-to-mass Z/A.

The data are obtained for 0, 2, 4, 6, 8 and 10 inches of the steel shield. The mean values of R for six materials are listed in Tab. 3 and the ratio curves are shown in Fig. 3.

TABLE II. DIFFERENT MATERIAL SLABS PLACEMENT

Looking to source:	Left	Center	Right
Above top shelf:		**DU**	
Top shelf:	**Al**		**Sn**
Bottom shelf:	**W**	**Fe**	**Pb**

Based on the look-up values the objects in the example image of Fig.2 are assigned colors for identified materials as exhibited on Fig. 4.

In the next experiment, we used objects of various size and shapes numbered in Fig.5. The objects are:
1: iron: width=1”, height = 1” and length = 5”
2: brass: diameter=3.5” and length = 2.2”
3: iron: width=1.8”, height = 1.5” and length=4.1”
4: iron: diameter = 2.5” and length = 8”
5: iron: width=1”, height = 1” and length = 7”
6: brass: width = 1”, height =1” and length = 17.1”

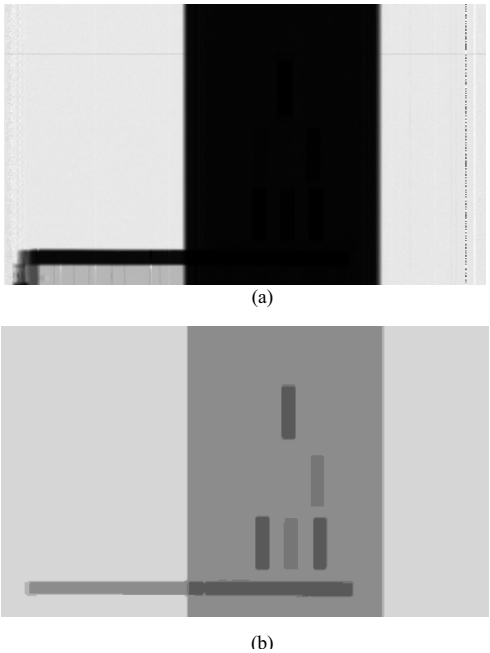

(a)

(b)

Figure 2. (a) 9MeV image with a 6” steel plate shield, (b) segmentation result.

TABLE III. MEAN RATIO, R

Shield	Al	Sn	W	Fe	Pb	DU
0”	0.928	0.950	1.013	0.871	0.999	1.035
2”	0.816	0.856	0.936	0.787	0.916	0.944
4”	0.732	0.770	0.880	0.713	0.833	0.895
6”	0.679	0.722	0.911	0.676	0.818	0.932
8”	0.646	0.748	1.036	0.679	0.869	1.077
10”	0.674	0.830	1.198	0.747	0.997	1.298

The attenuations have been measured in the test cell. The measurements are performed with a moving platform mimicking the projected speed of the cargo through the system, but in a vertical direction. The ratio values are obtained with a steel shield of 1.5” assuming this is a thickness and a material of a cargo container.

An image of these objects obtained at 9 MeV is demonstrated in Fig.6. One can notice a slight elongation caused by motion of the objects in vertical direction.

Next, we have performed an experiment by placing some of the above objects into the real cargo container loaded. The purpose of this experiment is to examine the resolution capability of the system. The test objects have been placed on the floor near the front wall (closer to the device).

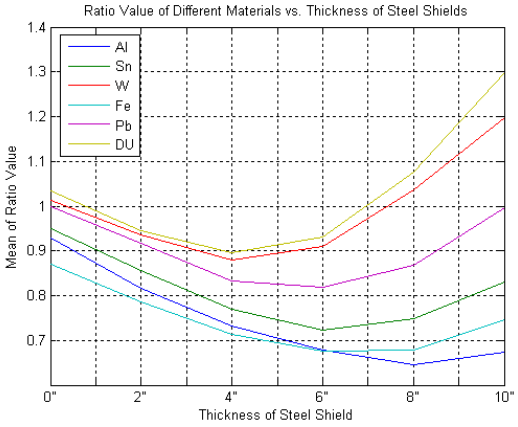

Figure 3. Ratio R, of different materials vs. thickness of steel shield.

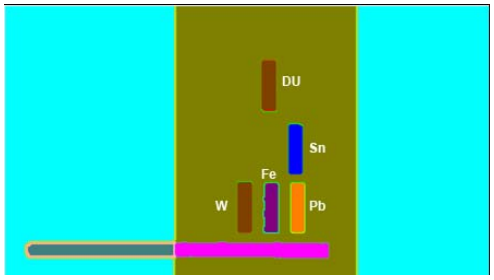

Figure 4. Material differentiation by look-up.

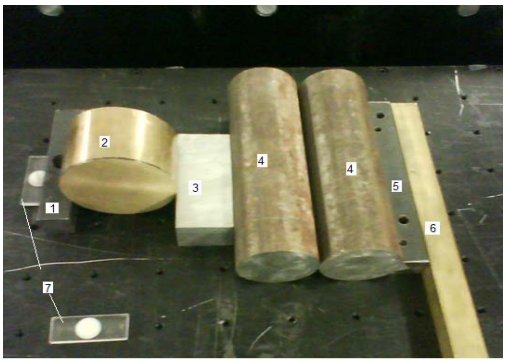

Figure 5. An experiment layout for shape, size and material analysis.

Figure 6. Objects of Fig.5 shined by 9 MeV.

The profiling method is applied for subtracting the container from the whole image in Fig.7a. This is done by identifying the "drops" in the profile functions in Fig. 7b, i.e. two global minima and one global minimum, respectively. The resulted signal is shown in Fig. 7c. A magnified region of interest is in Fig.8. The lower part of the image is relatively darker due to a slight slant of the platform towards the back. This creates an additional shielding effect on the lower part of the objects. The location of the objects is indicated by a rectangle in Fig.7c.

The segmentation of the intensity image makes objects apparent, and the following analysis of R and coloring shows "benign" materials for the objects found within the scene as shown in Figs. 9 and 10, respectively.

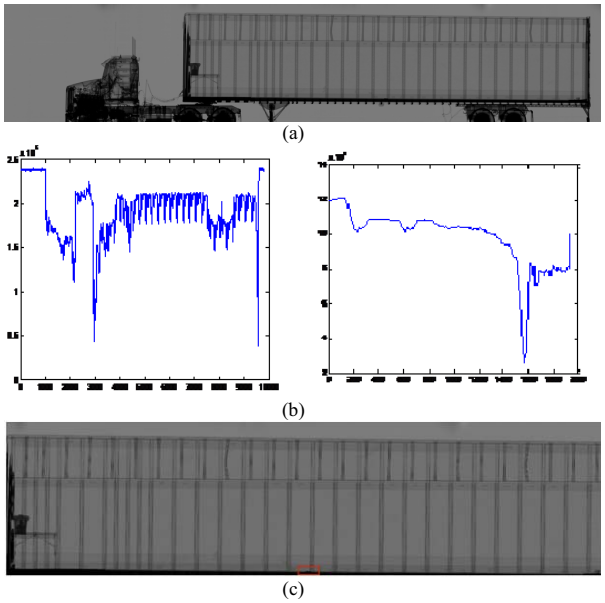

(a)

(b)

(c)

Figure 7. (a) Full image (32 bit); (b) vertical and horizontal profile functions; (c) subtracted container.

Figure 8. Suspicious region located.

Based on the ratio, R analysis, it is found that values derived from both the experimental setup and the real cargo container attenuation levels are approximately equal, that validates the methodology.

A Graphical User Interface (GUI) is developed for furnishing the technology with an interactive tool of processing, visualization and manipulating the images.

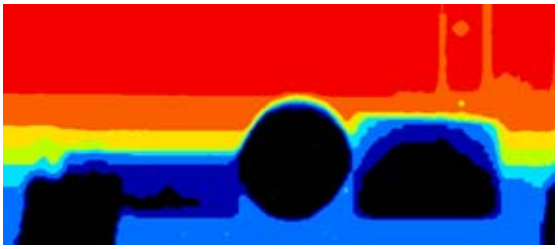

Figure 9. Segmentation of Fig.8 (a part)

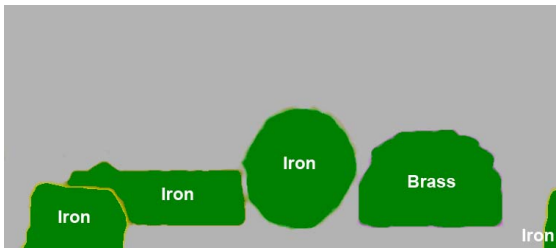

Figure 10. Coloring segmented objects of Fig.10 according to the look-up.

The GUI encapsulates the material identification algorithms with a minimal user involvement and also provides the means for the user to interact with the overall material detection process as for example, to define the number of classes, to zoom into a region of interest, or to outline a specific part of the image for processing. It has been implemented in a PC-Windows environment, using JAVA. The chosen software platform ensures maximum flexibility for the development and makes possible future porting to other environments, such as UNIX. More specific actions supported by the GUI are: (a) open, save or visualize partitions; (b) denoising based on wavelet shrinkage, median and morphological filtering; (c) logarithmic rescaling, contrast and brightness adjustment; (d) ratio, R calculation, segmentation; (e) pseudo coloring and material labeling.

IV. DISCUSSION

Although the technology is limited to identification of a single material behind a known barrier, i.e., container walls, it can be further extended. If a prior knowledge is available for the objects/materials in the container, the mixture of two or more materials can be also resolved. Since the mass attenuation of the mixture is a linear combination of the mass attenuations of composites weighted by the densities of each, a system of equations is capable to resolve the mixture cases as well. This needs the custom manifest reference. Instead, four levels of energies could be able to facilitate discrimination of two materials in the mix. Currently, the technology is available for three levels of interdigitation, and further developments are expected to enhance the mixture discrimination.

The preliminary studies have been conducted for complex scenes with irregular objects in overlay. The edge processing and shape analyses have been involved. The shape analysis is limited to detection of objects of axiosymmetric shapes, for example cylinders, cubes etc. The overall processing time is not exceeding the time of advancing the cargo through the system, i.e., 5 minutes. In fact it took three minutes to analyze a complex scene.

Quite small objects can be detected and their shapes are differentiated. It should be mentioned that there is a magnification effect depending on the position of the objects within the container, i.e. objects seen larger if they are closer to the wall facing the device. Although the experiments described in this paper have been limited to 10" of steel shield, the device is capable to penetrate through 17 inches of the material. We will continue with experimenting and complex scene to study the effect of adjacent materials on penetration levels and the scatter noise.

V. CONCLUSION

In this paper, we have introduced a system designed for inspecting cargo containers passing through the board. The major objective for the design is to facilitate the real-time inspection process. A practical time-limit is met and the technology is found feasible for identifying potential threats. The preliminary results show that the technology has a high potential for finding objects of the specified atomic numbers and shapes. Furthermore, the human operator can perform more efficiently on the enhanced images and with the assistance of the machine prompting. While a specific atomic number in an overlay cannot be identified accurately, suspicious regions can be located and reported. Beyond certain thicknesses of barriers, any suspicious attenuation which is non-adequate for the commercial cargo can be detected and reported. If a manifest of goods is available, found atomic numbers can be compared to reported ones. Further studies will be performed for evaluating true and false positive rates.

REFERENCES

[1] Varian Linatron Applications. available at http://www.varian.com/

[2] G. W. Philips, D. J. Nagel, and Timothy Coffey, "A Primer on the detection of nuclear and radiological weapons" (Washington, D.C.: Center for Technology and National Security Policy, National Defense University, July 2005), pp. 1-31, 46-47, 50-54

[3] J. Gormley, R. Richardson, V. Orphan, and E. Muenchau, "Advanced cargo container scanning technology development", Science Application International Corporation.

[4] P. J. Bjorkholm, "WMD detection", Cargo Security International. June/July 2005. Available at: http://www.varian.com/media/security_and_inspection/resources/articles/pdf/WMD_Detection.pdf

[5] S. Ogorodnikov and V. Petrunin, "Processing of interlaced images in 4-10 MeV dual energy customs system for material recognition". Physical Review Special Topics - Accelerators and Beams. Vol. 5, Issue 10, id. 104701, 2002

[6] V. Rebuffel and J. M. Dinten, "Dual-energy X-ray imaging: benefits and limits", Proc. 9th ECNDT, Berlin, September 2006.

[7] L. J. Schiff, Phys. Rev. 83, 252 (1951).

[8] E. Storm and H. Israel,''Photon cross section from 0.001 to 100 MeV for elements 1 through 100,'' Los Alamos Scientific Laboratory, New Mexico, 1967.

[9] V. L. Novikov, S. A. Ogorodnikov, and V. I. Petrunin, Problems of Atomic Science and Technology 4, 93 (1999), ISSN 1562-6016.